Published in final edited form as:
Exp Neurol. 2008 July ; 212(1): 100–107.

Brain Fiber Tract Plasticity in Experimental Spinal Cord Injury: Diffusion Tensor Imaging

Jaivijay Ramu[1], **Juan Herrera**[1], **Raymond Grill**[2], **Tobias Bockhorst**[1], and **Ponnada Narayana**[1,*]

1 *Department of Diagnostic and Interventional Imaging, University of Texas Medical School at Houston, 6431 Fannin Street, Houston, Texas 77030*

2 *Department of Neurosurgery, University of Texas Medical School at Houston, 6431 Fannin Street, Houston, Texas 77030*

Abstract

Diffusion tensor imaging (DTI) and immunohistochemistry were performed in spinal cord injured rats to understand the basis for activation of multiple regions in the brain observed in functional magnetic resonance imaging (fMRI) studies. The measured fractional anisotropy (FA), a scalar measure of diffusion anisotropy, along the region encompassing corticospinal tracts (CST) indicates significant differences between control and injured groups in the 3 to 4 mm area posterior to bregma that correspond to internal capsule and cerebral peduncle. Additionally, DTI-based tractography in injured animals showed increased number of fibers that extend towards the cortex terminating in the regions that were activated in fMRI. Both the internal capsule and cerebral peduncle demonstrated an increase in GFAP-immunoreactivity compared to control animals. GAP-43 expression also indicates plasticity in the internal capsule. These studies suggest that the previously observed multiple regions of activation in spinal cord injury are, at least in part, due to the formation of new fibers.

INTRODUCTION

Multiple imaging modalities have demonstrated cortical reorganization following spinal cord injury (SCI), both in humans and animals (Bruehlmeier, et al., 1998, Curt, et al., 2002, Jurkiewicz, et al., 2007, Lotze, et al., 2006, Nishimura, et al., 2007, Nowak, et al., 2005, Roelcke, et al., 1997). For example, functional magnetic resonance imaging (fMRI) has demonstrated reorganization of the corticospinal pathways and somatosensory cortex in response to the functional loss in both experimental and human SCI (Bareyre, et al., 2004, Bruehlmeier, et al., 1998, Hofstetter, et al., 2003, Raineteau and Schwab, 2001, Ramu, et al., 2007, Ramu, et al., 2006, Schallert, et al., 2000). In particular, recent fMRI studies identified activation of multiple areas in both cortical and deep gray matter structures in response to electrical stimulation of the forepaw in SCI animals, indicating greater brain activation compared to controls (Ramu, et al., 2007). The fMRI signal represents hemodynamic response that is closely associated with neural activity in response to a stimulus. The presence of multiple sites of activation on fMRI suggests any of the following: spontaneous generation of new pathways off of existing ones, reorganization of existing fibers, or unmasking of a latent pathways that previously existed (Donoghue, et al., 1990, Jacobs and Donoghue, 1991). An

*Corresponding Author: Tel: (713) 500-7677, Email: ponnada.a.narayana@uth.tmc.edu.

understanding of the reorganization mechanism(s) along with the factors that influence them may be helpful in the clinical management of SCI patients.

Diffusion tensor imaging (DTI) has the potential to non-invasively provide information about altered connectivity between different brain regions in response to SCI. DTI utilizes the directionality of water diffusion in tissue. The fiber structure within the white matter results in higher diffusion anisotropy relative to gray matter that is typically made of cell bodies with relatively little orientational preference. It is generally believed that the directionality or anisotropy in diffusion reflects the integrity of tissue microstructural reorganization. Diffusion anisotropy is determined both by the axonal structure and state of myelin (Beaulieu, 2002, Gulani, et al., 2001). Both damage to axonal structure and demyelination affect the observed anisotropy. Therefore, diffusion anisotropy can provide valuable information about altered white matter structure. The anisotropy or directionality of diffusion can be quantified by scalar quantities such as fractional anisotropy (FA). In addition, the longitudinal (λ_l) and transverse diffusivities (λ_t) that reflect water diffusion parallel and perpendicular to the directions to the fiber tracts can provide specific information about white matter pathology (Deo, et al., 2006, Gulani, et al., 2001, Herrera, et al., 2008, Schwartz, et al., 2005, Schwartz, et al., 2004, Song, et al., 2004, Song, et al., 2002). Additionally, information from the DTI measures can also be exploited to generate maps of the fiber tracts (see for example, (Nucifora, et al., 2007)). In this study we used DTI metrics along with the DTI-based fiber tracking and histology to investigate brain plasticity, fiber tract integrity and reorganization of ascending and descending pathways through the internal capsule and cerebral peduncle in SCI.

MATERIALS AND METHODS

Injury protocol

All procedures described in these studies were approved by our Institutional Animal Welfare Committee. The guidelines provided in NIH Guide for the Care and Use of Laboratory Animals was followed.

The DTI and histology studies were performed on the same group of animals on which the previous fMRI results have been reported (Ramu, et al., 2007). Adult male Sprague–Dawley rats weighing between 300 and 350g were used in these studies. A total of 12 rats were divided into 2 groups of six, each consisting of spinal cord injured and normal (uninjured) animals. The surgical procedure was performed as described previously (Ramu, et al., 2007). Briefly, after a laminectomy, a moderately severe contusive SCI was produced at the T7 level using the in-house-designed and fabricated injury device that has been shown to produce consistent injury (Narayana, et al., 2004). The control animals underwent laminectomy, but the spinal cords were uninjured.

Post-injury care

After injury animals received subcutaneous injection of Baytril (2.5 mg/kg, Bayer HealthCare LLC, Shawnee Mission, KS) for twice a day for 3 – 5 days. Buprenex (Reckitt Benckiser HealthCare Ltd., Hull, England) was also administered subcutaneously (0.01 mg/kg) twice a day for 5 days. Immediately after surgery, 5ml of saline was injected subcutaneously. Saline was administered twice daily for 5 days. Animals' bladders were expressed twice a day by the Crede method until spontaneous urination returned. Animals were weighed twice daily for the first week and every other day afterwards. Animals had free access to food and water.

Animal MRI Preparation

Animals underwent brain MRI at six weeks post injury. Animals were intubated and the anesthesia level was maintained by ventilating with a mixture of 2% isoflurane, 30% oxygen

and air through an endotracheal tube. The animals were placed on a Plexiglas bed secured with tooth and ear bars. The respiration and rectal temperature were monitored throughout the experiment with a MR compatible physiologic monitoring unit (Model 1025, SA Instruments, Inc., Stonybrook, NY). The Nonin pulse oximeter (Model 8600V) was used to monitor heart rate and oxygen levels. For the duration of the experiment, the SA Heating System (Model 11007B, SA Instruments, Inc., Stonybrook, NY) was used to maintain the l body temperature at 37 °C.

MR image acquisitions

All MR studies were performed on a USR70/30 horizontal bore 7T MR Scanner Bruker Biospin, Karlsruhe, Germany). A 71 mm diameter birdcage resonator was used for radio frequency (RF) transmission, and an actively decoupled quadrature surface coil was used for signal reception (Ramu, et al., 2006). High-resolution anatomical RARE images were acquired using the following parameters: rare factor of 4, TR/TE of 5000 ms/68.4 ms, image matrix of 256 × 256, field of view 3.84 cm × 3.84 cm, and 20 contiguous, 1mm thick slices. DTI images were acquired with identical geometry as the anatomical images using a multi-shot spin echo EPI sequence (number of shots 4) with TR/TE of 3000 ms/38.3 ms, b factor of 1000 sec mm^{-2} (gradient amplitude of 366 mT/m), bandwidth of 200 kHz, 42 gradient encoding directions (Madi, et al., 2005), acquisition matrix of 128 × 128, and field of view 3.84 cm × 3.84 cm. DTI images were reconstructed to 256 × 256 matrix.

DTI Analysis

All the diffusion weighted images were registered to the rat brain in stereotaxic coordinates (Paxinos and Watson, 2005) using the Automated Image Registration (Woods, et al., 1998) as described elsewhere (Ramu, et al., 2006). These images were then imported into DTI Studio software (Jiang, et al., 2006) to calculate the DTI parameters such as fractional anisotropy (FA), mean diffusivity (MD), and eigenvalue maps.

Fractional Anisotropy (FA) t-test

After registration to the rat brain in stereotaxic coordinate system (Paxinos and Watson, 2005), the individual FA maps of the normal-uninjured and the six weeks post-injury animals were generated using DTI studio (Jiang, et al., 2006) and were then averaged. A two-sample statistical t-test ($P < 0.05$) was performed using SPM99 (Wellcome Department of Imaging Neuroscience, UCL, London) for unbiased determination of the significant differences in the FA values between the injured and normal animals. Maps of these significant differences were generated (t-maps).

FA Region of Interest (ROI) Analysis

The ROI analysis of FA maps was performed using DTI studio (Jiang, et al., 2006) to verify that the t-maps correctly identified the regions with significant FA differences. Elliptical ROIs were used with the major axis of 8 mm and minor axis of 4 mm along the corticospinal tract (CST). The FA values were also measured in different regions along the CST starting at bregma -13 to bregma -3 to ascertain the absence of significant differences in other regions on these tracts. The same set of ROIs was used to determine the FA values for both normal-uninjured and six weeks post injury groups.

Fiber tracking

Fiber tracking was performed based on Fiber Assignment by Continuous Tracking (FACT) algorithm (Mori, et al., 1999) using the DTI studio (Jiang, et al., 2006). ROIs were drawn to trace the CST with an FA threshold of 0.16 and an angle threshold 60° based on the photographic atlas of the rat brain (Kruger, et al., 1995). Once the CST was traced based on a

normal-uninjured rat, the same set of ROIs was used to trace the CST in the injured rats. The fiber count and FA along the fibers were also determined.

Histology

Following the terminal MRI scans, animals were transcardially perfused with saline followed by 4% paraformaldehyde (PFA). The brain was then removed, post-fixed overnight in 4% PFA, and then immersed in 30% sucrose-phosphate buffered saline (0.1M PBS) for 2–3 days at 4 °C. The brain was sectioned coronally at a section thickness of 40 μm using a cryostat (Leica CM1800, Bannockburn, IL) and stored at −20 °C in tissue storing media.

Brain sections were processed as free floating and were incubated in the following primary antibodies: myelin basic protein (MBP; Millipore, Billerica, MA), neurofilament-heavy protein (NF-H; Millipore, Billerica, MA), GAP-43 (Millipore, Billerica, MA) and glial fibrillary acidic protein (GFAP; Millipore, Billerica, MA). Primary antibodies were diluted with blocking solution (0.1M PBS containing 5% goat serum and 0.3% Triton X-100). For controls, only secondary antibodies were applied to determine antibody specificity.

Appropriate secondary antibodies were used at a dilution of 1:500 in 0.1M PBS. The following Alexafluor® dye conjugated secondary antibodies were used: goat anti-mouse IgG Alexa Fluor® 488 (Invitrogen, Carlsbad, CA) and goat anti-rabbit IgG (H+L) Alex Fluor® 568 (Invitrogen, Carlsbad, CA). Tissue sections were viewed and captured using a Spot Flex digital camera (Diagnostic Instruments, Inc. Sterling Heights, MI) attached to a Leica RX1500 upright microscope and the images were collected using Spot software (Diagnostic Imaging, Sterling Heights, MI). The operator acquiring the images was blinded to the groups.

Histology Analysis

Quantitative analysis was performed using ImagePro Plus software (Media Cybernetics, Inc.; Silver Spring, MD). Free floating brain sections (n=10 sections/animal) were used in quantification of the percent areas or fluorescent intensities of myelin, neurofilament, GAP-43, and GFAP in the defined ROI. Using the predefined threshold levels from normal brain sections the fluorescent intensities were determined in both groups. In order to correlate DTI and histology, the ROIs were drawn in the internal capsule and cerebral peduncle regions that were affected based on the t-maps. All the ROIs had approximately the same size (a sphere with a 200 μm diameter).

Statistical Analysis

The Mann-Whitney Rank Sum Test was used to determine differences in the percent of expression of myelin, neurofilament, GAP-43 and GFAP in the respective ROIs. Statistical analysis was performed using GraphPad Prism4 software (GraphPad Software, San Diego, CA). Significance levels were set at $P = 0.05$ for all comparisons.

RESULTS

Fig. 1 shows the FA maps along with the RGB color-coding representing the fiber orientation of a normal animal at the level of 0.2 mm (Fig. 1a) and 2.7 mm (Fig. 1b) posterior to bregma. In this figure, the colors represent fiber orientation (red: left - right, green: ventral – dorsal, blue: rostral – caudal) and the intensity indicates the FA value. The t-maps (shown in green) which represent the significant group differences in the FA values between the normal and injured groups superimposed on the FA maps are shown in Fig. 2 (images from left to right are at levels 3.2 mm, 2.8 mm, 2.4 mm posterior to bregma, respectively). As can be seen on this figure, significant differences were observed in the cerebral peduncle and the internal capsule regions.

In these studies we examined the CST. The DTI-based CST fiber tracts superimposed on the sagittal MR image of a rat brain are shown in Fig. 3a. The CST was traced by drawing the ROIs using DTI Studio (Jiang, et al., 2006) on axial slices of the brain with the aid of Paxinos and Watson rat brain atlas (Paxinos and Watson, 2005). For comparison, a biotinylated dextran (BDA) CST traced brain from a separate study was used to verify that the regions encompassing the DTI fiber tracts contained CST fibers in the internal capsule (Fig. 3b) and cerebral peduncle (Fig. 3b). The BDA tracing was generated on a normal animal using the procedure described elsewhere (Grill, et al., 1997). The colors on the tractography shown in Fig. 3a indicate fibers originating from different seed points used for generating the fiber maps (tractography) to aid in the visualization and do not indicate fiber directionality. For comparison, the fiber maps in a normal and six weeks post-injured rats are illustrated in Fig. 4a and Fig. 4b, respectively. The measured FA values along the CST shown in Fig. 4c indicate significant differences between the control and injured groups only in the 3 to 4 mm region posterior to bregma. These regions correspond to the internal capsule and cerebral peduncle. Additionally, fibers from injured animals extended towards the cortex terminating in the regions that were activated in fMRI (Ramu, et al., 2007). Results from the statistical analysis of the differences in the fiber count and FA values in the internal capsule and the cerebral peduncle regions are shown in Fig. 5. In the internal capsule and cerebral peduncles there was a significant increase (**$P < 0.05$**) in the fiber counts in the six weeks post-injured group relative to the uninjured group (Fig. 5a), which was consistent with the visual inspection. There was also significant increase (**$P < 0.05$**) in the same regions in the FA values in the six weeks post-injured group compared to the uninjured group (Fig. 5b). Also the longitudinal (λ_l) and transverse diffusivities (λ_t) did not show significant differences within the internal capsule between the injured and control groups. However, in the cerebral peduncle a significant difference was observed in λ_t (Table 1). A trend towards decreased λ_l in the injured group was also observed in the cerebral peduncle.

In order to understand the pathologic substrate underlying the DTI – observed changes in λ_l and λ_t in the internal capsule and cerebral peduncle, we used immunohistology to identify axons and myelin using antibodies against the heavy chain of neurofilament and myelin, respectively. We detected a significant decrease in the amount of myelin and neurofilament in the internal capsule of injured subjects. No such changes in immunolabeling were found in the cerebral peduncle. To determine if the DTI-observed increase in fiber count can be attributed to axonal sprouting, we examined the tissue for the expression of GAP-43, a marker of axonal growth and/or sprouting (Skene, et al., 1986). Quantification of GAP-43 immunohistochemistry demonstrated a significant increase that was localized to the internal capsule, but not the cerebral peduncle (Fig. 6). We further examined brain sections for glial fibrillary acidic protein (GFAP) expression. GFAP has also been thought to play a role in affecting the DTI measures (Harsan, et al., 2007). Both the internal capsule and cerebral peduncle demonstrated an increase in GFAP-immunoreactivity compared to control animals.

DISCUSSION

Previous fMRI studies have shown multiple areas of activation when an unaffected limb was stimulated following spinal cord injury (Ramu, et al., 2007, Ramu, et al., 2006). This is different from normal uninjured animals showing a single activated region in the somatosensory cortex in response to the same stimuli. This study attempts to understand and determine if fiber reorganization/regeneration can account for the increased brain activation following spinal cord injury. Our DTI-based tractography indicates the presence of new fibers in the SCI animals. These new fibers pass through a number of deep gray matter structures and terminate in the same the cortical regions that were activated in the fMRI studies. These new fibers presumably provide the functional/anatomical connectivity between different structures and would explain the greater activation observed on fMRI in injured animals relative to controls. In addition, the increased FA value is consistent with the formation of these new connections.

Synaptic unmasking of previously present but functionally inactive connections (Donoghue, et al., 1990, Jacobs and Donoghue, 1991) may also play a role in the increase in FA and fiber count. Whatever the mechanism might be, our studies demonstrate significant fiber tract reorganization in response to spinal cord injury.

Our DTI results suggest that significant reorganization occurs only in internal capsule and cerebral peduncles when assessed at 6 weeks post-SCI. These two structures contain compact bundles of afferent and efferent fibers that form connections between the cortex, thalamus, basal ganglia, brainstem, and spinal cord (Cowan and de Vries, 2005). Specifically, corticopontine fibers that connect frontal cortex to the pons are found in the anterior internal capsule whereas descending corticospinal and sensory fibers comprise the posterior component of the internal capsule (Gilman, et al., 1996), while the cerebral peduncles contain mainly descending corticopontine and corticospinal fibers. Combined, these tracts are implicated in the planning and initiating of movements, coordinating fine motor movements, and conveying sensory information.

The concept of cortical reorganization following SCI has been explored through a range of both invasive and non-invasive techniques that show considerable alterations in both human and rat brain activity resulting from SCI (Endo, et al., 2007, Lotze, et al., 2006, Lotze, et al., 1999, Ramu, et al., 2007, Winchester, et al., 2005). Previous studies have indicated that injury-induced changes can occur at the molecular level as evidenced by alterations in the expression of sodium channels both within the spinal cord and at the level of the thalamus following SCI which may underline the onset and maintenance of neuropathic pain (Hains, et al., 2003, Hains, et al., 2005, Hains and Waxman, 2007). Such alterations both within the cord and in supraspinal projections may give rise to functional improvements and also provide targets for novel interventions to promote plasticity and functional improvement (Bareyre, et al., 2004, Maier and Schwab, 2006, Raineteau, et al., 2002). Reorganization in supraspinal projections has been shown to be enhanced following the delivery of white-matter inhibitors in several rodent CNS models including SCI (Emerick, et al., 2003), cortical lesion (Emerick, et al., 2003, Kartje, et al., 1999), stroke (Markus, et al., 2005, Papadopoulos, et al., 2002, Papadopoulos, et al., 2006, Seymour, et al., 2005). However, our current study indicates that substantial reorganization occurs in sub-cortical targets even in the absence of such targeted interventions.

A number of factors contribute to the observed changes in the DTI metrics in our study. These include increased myelination, altered axonal morphology, and increased fiber density due to new sprouting, as mentioned earlier. In order to non-invasively tease out the contributions of these various components to the observed changes in the FA values, we have determined the individual diffusivities λ_l and λ_t. For example, correlation between individual diffusivities and axonal integrity and myelination has been previously demonstrated in conditions of ischemic stroke (Thomalla, et al., 2004), optic nerve injury (Song, et al., 2003, Song, et al., 2002), and a mouse model of myelin deficiency (Nair, et al., 2005). Based on the current studies, the DTI measures λ_l, and λ_t showed little correlation to the histological labeling of neurofilament and myelin in either the internal capsule or cerebral peduncle. DeBoy et al., (DeBoy, et al., 2007) recently showed in experimental autoimmune encephalomyelitis, an experimental model of multiple sclerosis, absence of correlation between myelin content and λ_t values. In a recent study by Herrera et al., (Herrera, et al., 2008) demonstrated discrepancies between DTI measures and histology following spinal cord injury. It appears that correlating individual diffusivities with brain histology in spinal cord injury is complex. Our data suggests that other cell populations, apart from the neuronal and oligodendrocyte populations also might influence the DTI measures.

Another contributing factor to the DTI measures could be the astrocytic response to injury, which has previously been suggested to influence the FA values (Harsan, et al., 2007). Harsan

et al., (Harsan, et al., 2007) showed in jimpy mice, a model of Pelizaeus-Merzbacher diseases (PMD), that astrocytic hypertrophy influences diffusivity measures. The observed increase in GFAP expression may indicate the astrocytic response to injury where a hallmark of reactive astrocytes is hypertrophy. Astrocytic processes might influence water diffusion coefficients because they interact and follow the axonal pathway longitudinally (Skoff, 1976). Additionally, astrocytes also play a major role as regulators of water homeostasis by the expression of aquaporins (Amiry-Moghaddam, et al., 2004, Amiry-Moghaddam, et al., 2003). Aquaporins are a family of at least 11 homologous water channel proteins that provide the major route for water movement in all tissues, including the nervous system (Amiry-Moghaddam, et al., 2003, Badaut, et al., 2002, Manley, et al., 2004, Manley, et al., 2000). Astrocytic aquaporin-4 expression has been shown to significantly increase after spinal cord injury (Nesic, et al., 2006).

Reactive astrocytes, which classically viewed as inhibitory to regeneration (Ribotta, et al., 2004), have also been reported to express molecules that may support and encourage such plasticity (Aubert, et al., 1998, Camand, et al., 2004, Dusart, et al., 1999). Thus, it would be improper to assess a particular contribution of reactive astrocytes to observed alterations in FA values without a more detailed analysis of the nature of the glial reactivity, i.e., co-localization with growth-associated molecules or permissive cell surface and/or extracellular matrix molecules.

These studies investigated the DTI changes at only six-week time point. The rationale for this time point was that our previous fMRI study clearly demonstrated multiple activation sites around this time point (Ramu, et al., 2007). Thus our studies do not allow any conclusions to be drawn about the earliest onset of demonstrable fiber tract plasticity. Even though the animals did not show any ill effects at the end of the scan, we were concerned about the long-term effects of α-chloralose on the animals. For example, repeated exposure to α-chloralose could result in organ failure (Weber, et al., 2005). Thus these studies do not truly represent longitudinal investigations. True longitudinal studies are critical for objectively evaluating plasticity. Finally, since the main focus of these studies was to investigate the plasticity using noninvasive imaging technology, we have not investigated in detail the effect of plasticity on the neurobehavioral and neurosensory outcomes. We plan to address all these issues in our ongoing studies.

Acknowledgements

This work is supported by NIH grants R01 NS30821 and NS045624 awarded to PAN. We thank Shi-Je Liu, MD for surgical manipulation of the animals and Tessy Chacko, BS, and Alex Li, BS for their help with histology.

References

1. Amiry-Moghaddam M, Frydenlund DS, Ottersen OP. Anchoring of aquaporin-4 in brain: molecular mechanisms and implications for the physiology and pathophysiology of water transport. Neuroscience 2004;129:999–1010. [PubMed: 15561415]
2. Amiry-Moghaddam M, Otsuka T, Hurn PD, Traystman RJ, Haug FM, Froehner SC, Adams ME, Neely JD, Agre P, Ottersen OP, Bhardwaj A. An alpha-syntrophin-dependent pool of AQP4 in astroglial end-feet confers bidirectional water flow between blood and brain. Proc Natl Acad Sci U S A 2003;100:2106–2111. [PubMed: 12578959]
3. Aubert I, Ridet JL, Schachner M, Rougon G, Gage FH. Expression of L1 and PSA during sprouting and regeneration in the adult hippocampal formation. J Comp Neurol 1998;399:1–19. [PubMed: 9725697]
4. Badaut J, Lasbennes F, Magistretti PJ, Regli L. Aquaporins in brain: distribution, physiology, and pathophysiology. J Cereb Blood Flow Metab 2002;22:367–378. [PubMed: 11919508]

5. Bareyre FM, Kerschensteiner M, Raineteau O, Mettenleiter TC, Weinmann O, Schwab ME. The injured spinal cord spontaneously forms a new intraspinal circuit in adult rats. Nat Neurosci 2004;7:269–277. [PubMed: 14966523]
6. Beaulieu C. The basis of anisotropic water diffusion in the nervous system - a technical review. NMR Biomed 2002;15:435–455. [PubMed: 12489094]
7. Bruehlmeier M, Dietz V, Leenders KL, Roelcke U, Missimer J, Curt A. How does the human brain deal with a spinal cord injury? Eur J Neurosci 1998;10:3918–3922. [PubMed: 9875370]
8. Camand E, Morel MP, Faissner A, Sotelo C, Dusart I. Long-term changes in the molecular composition of the glial scar and progressive increase of serotoninergic fibre sprouting after hemisection of the mouse spinal cord. Eur J Neurosci 2004;20:1161–1176. [PubMed: 15341588]
9. Cowan FM, de Vries LS. The internal capsule in neonatal imaging. Seminars in fetal & neonatal medicine 2005;10:461–474. [PubMed: 16002354]
10. Curt A, Alkadhi H, Crelier GR, Boendermaker SH, Hepp-Reymond MC, Kollias SS. Changes of non-affected upper limb cortical representation in paraplegic patients as assessed by fMRI. Brain 2002;125:2567–2578. [PubMed: 12390981]
11. DeBoy CA, Zhang J, Dike S, Shats I, Jones M, Reich DS, Mori S, Nguyen T, Rothstein B, Miller RH, Griffin JT, Kerr DA, Calabresi PA. High resolution diffusion tensor imaging of axonal damage in focal inflammatory and demyelinating lesions in rat spinal cord. Brain 2007;130:2199–2210. [PubMed: 17557778]
12. Deo AA, Grill RJ, Hasan KM, Narayana PA. In vivo serial diffusion tensor imaging of experimental spinal cord injury. J Neurosci Res 2006;83:801–810. [PubMed: 16456864]
13. Donoghue JP, Suner S, Sanes JN. Dynamic organization of primary motor cortex output to target muscles in adult rats. II. Rapid reorganization following motor nerve lesions. Exp Brain Res 1990;79:492–503. [PubMed: 2340869]
14. Dusart I, Morel MP, Wehrle R, Sotelo C. Late axonal sprouting of injured Purkinje cells and its temporal correlation with permissive changes in the glial scar. J Comp Neurol 1999;408:399–418. [PubMed: 10340514]
15. Emerick AJ, Neafsey EJ, Schwab ME, Kartje GL. Functional reorganization of the motor cortex in adult rats after cortical lesion and treatment with monoclonal antibody IN-1. J Neurosci 2003;23:4826–4830. [PubMed: 12832504]
16. Endo T, Spenger C, Tominaga T, Brené S, Olson L. Cortical sensory map rearrangement after spinal cord injury: fMRI responses linked to Nogo signalling. Brain. 2007
17. Gilman, S.; Newman, SW.; Manter, JT.; Gatz, AJ. Manter and Gatz's essentials of clinical neuroanatomy and neurophysiology. F.A. Davis; Philadelphia: 1996.
18. Grill R, Murai K, Blesch A, Gage FH, Tuszynski MH. Cellular delivery of neurotrophin-3 promotes corticospinal axonal growth and partial functional recovery after spinal cord injury. J Neurosci 1997;17:5560–5572. [PubMed: 9204937]
19. Gulani V, Webb AG, Duncan ID, Lauterbur PC. Apparent diffusion tensor measurements in myelin-deficient rat spinal cords. Magn Reson Med 2001;45:191–195. [PubMed: 11180424]
20. Hains BC, Klein JP, Saab CY, Craner MJ, Black JA, Waxman SG. Upregulation of sodium channel Nav1.3 and functional involvement in neuronal hyperexcitability associated with central neuropathic pain after spinal cord injury. J Neurosci 2003;23:8881–8892. [PubMed: 14523090]
21. Hains BC, Saab CY, Waxman SG. Changes in electrophysiological properties and sodium channel Nav1.3 expression in thalamic neurons after spinal cord injury. Brain 2005;128:2359–2371. [PubMed: 16109750]
22. Hains BC, Waxman SG. Sodium channel expression and the molecular pathophysiology of pain after SCI. Prog Brain Res 2007;161:195–203. [PubMed: 17618978]
23. Harsan LA, Poulet P, Guignard B, Parizel N, Skoff RP, Ghandour MS. Astrocytic hypertrophy in dysmyelination influences the diffusion anisotropy of white matter. J Neurosci Res 2007;85:935–944. [PubMed: 17278151]
24. Herrera JJ, Chacko T, Narayana PA. Histological correlation of diffusion tensor imaging metrics in experimental spinal cord injury. J Neurosci Res 2008;86:443–447. [PubMed: 17868152]

25. Hofstetter CP, Schweinhardt P, Klason T, Olson L, Spenger C. Numb rats walk - a behavioural and fMRI comparison of mild and moderate spinal cord injury. Eur J Neurosci 2003;18:3061–3068. [PubMed: 14656301]
26. Jacobs KM, Donoghue JP. Reshaping the cortical motor map by unmasking latent intracortical connections. Science 1991;251:944–947. [PubMed: 2000496]
27. Jiang H, van Zijl PC, Kim J, Pearlson GD, Mori S. DtiStudio: resource program for diffusion tensor computation and fiber bundle tracking. Comput Methods Programs Biomed 2006;81:106–116. [PubMed: 16413083]
28. Jurkiewicz MT, Mikulis DJ, McIlroy WE, Fehlings MG, Verrier MC. Sensorimotor cortical plasticity during recovery following spinal cord injury: a longitudinal FMRI study. Neurorehabil Neural Repair 2007;21:527–538. [PubMed: 17507643]
29. Kartje GL, Schulz MK, Lopez-Yunez A, Schnell L, Schwab ME. Corticostriatal plasticity is restricted by myelin-associated neurite growth inhibitors in the adult rat. Ann Neurol 1999;45:778–786. [PubMed: 10360770]
30. Kruger, L.; Saporta, S.; Swanson, LW. PhotographicAtlas of the Rat Brain. Cambridge University Press; Cambridge CB2 1RP: 1995.
31. Lotze M, Laubis-Herrmann U, Topka H. Combination of TMS and fMRI reveals a specific pattern of reorganization in M1 in patients after complete spinal cord injury. Restor Neurol Neurosci 2006;24:97–107. [PubMed: 16720945]
32. Lotze M, Laubis-Herrmann U, Topka H, Erb M, Grodd W. Reorganization in the primary motor cortex after spinal cord injury - A functional Magnetic Resonance (fMRI) study. Restor Neurol Neurosci 1999;14:183–187. [PubMed: 12671262]
33. Madi S, Hasan KM, Narayana PA. Diffusion tensor imaging of in vivo and excised rat spinal cord at 7 T with an icosahedral encoding scheme. Magn Reson Med 2005;53:118–125. [PubMed: 15690510]
34. Maier IC, Schwab ME. Sprouting, regeneration and circuit formation in the injured spinal cord: factors and activity. Philos Trans R Soc Lond, B, Biol Sci 2006;361:1611–1634. [PubMed: 16939978]
35. Manley GT, Binder DK, Papadopoulos MC, Verkman AS. New insights into water transport and edema in the central nervous system from phenotype analysis of aquaporin-4 null mice. Neuroscience 2004;129:983–991. [PubMed: 15561413]
36. Manley GT, Fujimura M, Ma T, Noshita N, Filiz F, Bollen AW, Chan P, Verkman AS. Aquaporin-4 deletion in mice reduces brain edema after acute water intoxication and ischemic stroke. Nat Med 2000;6:159–163. [PubMed: 10655103]
37. Markus TM, Tsai SY, Bollnow MR, Farrer RG, O'Brien TE, Kindler-Baumann DR, Rausch M, Rudin M, Wiessner C, Mir AK, Schwab ME, Kartje GL. Recovery and brain reorganization after stroke in adult and aged rats. Ann Neurol 2005;58:950–953. [PubMed: 16315284]
38. Mori S, Crain BJ, Chacko VP, van Zijl PC. Three-dimensional tracking of axonal projections in the brain by magnetic resonance imaging. Ann Neurol 1999;45:265–269. [PubMed: 9989633]
39. Nair G, Tanahashi Y, Low HP, Billings-Gagliardi S, Schwartz WJ, Duong TQ. Myelination and long diffusion times alter diffusion-tensor-imaging contrast in myelin-deficient shiverer mice. Neuroimage 2005;28:165–174. [PubMed: 16023870]
40. Narayana PA, Grill RJ, Chacko T, Vang R. Endogenous recovery of injured spinal cord: longitudinal in vivo magnetic resonance imaging. J Neurosci Res 2004;78:749–759. [PubMed: 15499591]
41. Nesic O, Lee J, Ye Z, Unabia GC, Rafati D, Hulsebosch CE, Perez-Polo JR. Acute and chronic changes in aquaporin 4 expression after spinal cord injury. Neuroscience 2006;143:779–792. [PubMed: 17074445]
42. Nishimura Y, Onoe H, Morichika Y, Perfiliev S, Tsukada H, Isa T. Time-dependent central compensatory mechanisms of finger dexterity after spinal cord injury. Science 2007;318:1150–1155. [PubMed: 18006750]
43. Nowak M, Holm S, Biering-Sorensen F, Secher NH, Friberg L. Central command" and insular activation during attempted foot lifting in paraplegic humans. Hum Brain Mapp 2005;25:259–265. [PubMed: 15849712]
44. Nucifora PG, Verma R, Lee SK, Melhem ER. Diffusion-tensor MR imaging and tractography: exploring brain microstructure and connectivity. Radiology 2007;245:367–384. [PubMed: 17940300]

45. Papadopoulos CM, Tsai SY, Alsbiei T, O'Brien TE, Schwab ME, Kartje GL. Functional recovery and neuroanatomical plasticity following middle cerebral artery occlusion and IN-1 antibody treatment in the adult rat. Ann Neurol 2002;51:433–441. [PubMed: 11921049]
46. Papadopoulos CM, Tsai SY, Cheatwood JL, Bollnow MR, Kolb BE, Schwab ME, Kartje GL. Dendritic plasticity in the adult rat following middle cerebral artery occlusion and Nogo-a neutralization. Cereb Cortex 2006;16:529–536. [PubMed: 16033928]
47. Paxinos, G.; Watson, C. The Rat Brain in Stereotaxic Coordinates. Elsevier Academic Press; Burlington, MA, USA: 2005.
48. Raineteau O, Fouad K, Bareyre FM, Schwab ME. Reorganization of descending motor tracts in the rat spinal cord. Eur J Neurosci 2002;16:1761–1771. [PubMed: 12431229]
49. Raineteau O, Schwab ME. Plasticity of motor systems after incomplete spinal cord injury. Nat Rev Neurosci 2001;2:263–273. [PubMed: 11283749]
50. Ramu J, Bockhorst KH, Grill RJ, Mogatadakala KV, Narayana PA. Cortical reorganization in NT3-treated experimental spinal cord injury: Functional magnetic resonance imaging. Exp Neurol 2007;204:58–65. [PubMed: 17112518]
51. Ramu J, Bockhorst KH, Mogatadakala KV, Narayana PA. Functional magnetic resonance imaging in rodents: Methodology and application to spinal cord injury. J Neurosci Res 2006;84:1235–1244. [PubMed: 16941500]
52. Ribotta MG, Menet V, Privat A. Glial scar and axonal regeneration in the CNS: lessons from GFAP and vimentin transgenic mice. Acta Neurochir Suppl 2004;89:87–92. [PubMed: 15335106]
53. Roelcke U, Curt A, Otte A, Missimer J, Maguire RP, Dietz V, Leenders KL. Influence of spinal cord injury on cerebral sensorimotor systems: a PET study. J Neurol Neurosurg Psychiatry 1997;62:61–65. [PubMed: 9010401]
54. Schallert T, Fleming SM, Leasure JL, Tillerson JL, Bland ST. CNS plasticity and assessment of forelimb sensorimotor outcome in unilateral rat models of stroke, cortical ablation, parkinsonism and spinal cord injury. Neuropharmacology 2000;39:777–787. [PubMed: 10699444]
55. Schwartz ED, Chin CL, Shumsky JS, Jawad AF, Brown BK, Wehrli S, Tessler A, Murray M, Hackney DB. Apparent diffusion coefficients in spinal cord transplants and surrounding white matter correlate with degree of axonal dieback after injury in rats. AJNR American journal of neuroradiology 2005;26:7–18. [PubMed: 15661691]
56. Schwartz ED, Cooper ET, Fan Y, Jawad AF, Chin CL, Nissanov J, Hackney DB. MRI diffusion coefficients in spinal cord correlate with axon morphometry. Neuroreport 2004;16:73–76. [PubMed: 15618894]
57. Seymour AB, Andrews EM, Tsai SY, Markus TM, Bollnow MR, Brenneman MM, O'Brien TE, Castro AJ, Schwab ME, Kartje GL. Delayed treatment with monoclonal antibody IN-1 1 week after stroke results in recovery of function and corticorubral plasticity in adult rats. J Cereb Blood Flow Metab 2005;25:1366–1375. [PubMed: 15889044]
58. Skene JH, Jacobson RD, Snipes GJ, McGuire CB, Norden JJ, Freeman JA. A protein induced during nerve growth (GAP-43) is a major component of growth-cone membranes. Science 1986;233:783–786. [PubMed: 3738509]
59. Skoff RP. Myelin deficit in the Jimpy mouse may be due to cellular abnormalities in astroglia. Nature 1976;264:560–562. [PubMed: 1004595]
60. Song SK, Kim JH, Lin SJ, Brendza RP, Holtzman DM. Diffusion tensor imaging detects age-dependent white matter changes in a transgenic mouse model with amyloid deposition. Neurobiol Dis 2004;15:640–647. [PubMed: 15056472]
61. Song SK, Sun SW, Ju WK, Lin SJ, Cross AH, Neufeld AH. Diffusion tensor imaging detects and differentiates axon and myelin degeneration in mouse optic nerve after retinal ischemia. Neuroimage 2003;20:1714–1722. [PubMed: 14642481]
62. Song SK, Sun SW, Ramsbottom MJ, Chang C, Russell J, Cross AH. Dysmyelination revealed through MRI as increased radial (but unchanged axial) diffusion of water. Neuroimage 2002;17:1429–1436. [PubMed: 12414282]
63. Thomalla G, Glauche V, Koch MA, Beaulieu C, Weiller C, Röther J. Diffusion tensor imaging detects early Wallerian degeneration of the pyramidal tract after ischemic stroke. Neuroimage 2004;22:1767–1774. [PubMed: 15275932]

64. Weber R, Ramos-Cabrer P, Wiedermann D, van Camp N, Hoehn M. A fully noninvasive and robust experimental protocol for longitudinal fMRI studies in the rat. Neuroimage. 2005

65. Winchester P, McColl R, Querry R, Foreman N, Mosby J, Tansey K, Williamson J. Changes in Supraspinal Activation Patterns following Robotic Locomotor Therapy in Motor-Incomplete Spinal Cord Injury. Neurorehabil Neural Repair 2005;19:313–324. [PubMed: 16263963]

66. Woods RP, Grafton ST, Holmes CJ, Cherry SR, Mazziotta JC. Automated image registration: I. General methods and intrasubject, intramodality validation. J Comput Assist Tomogr 1998;22:139–152. [PubMed: 9448779]

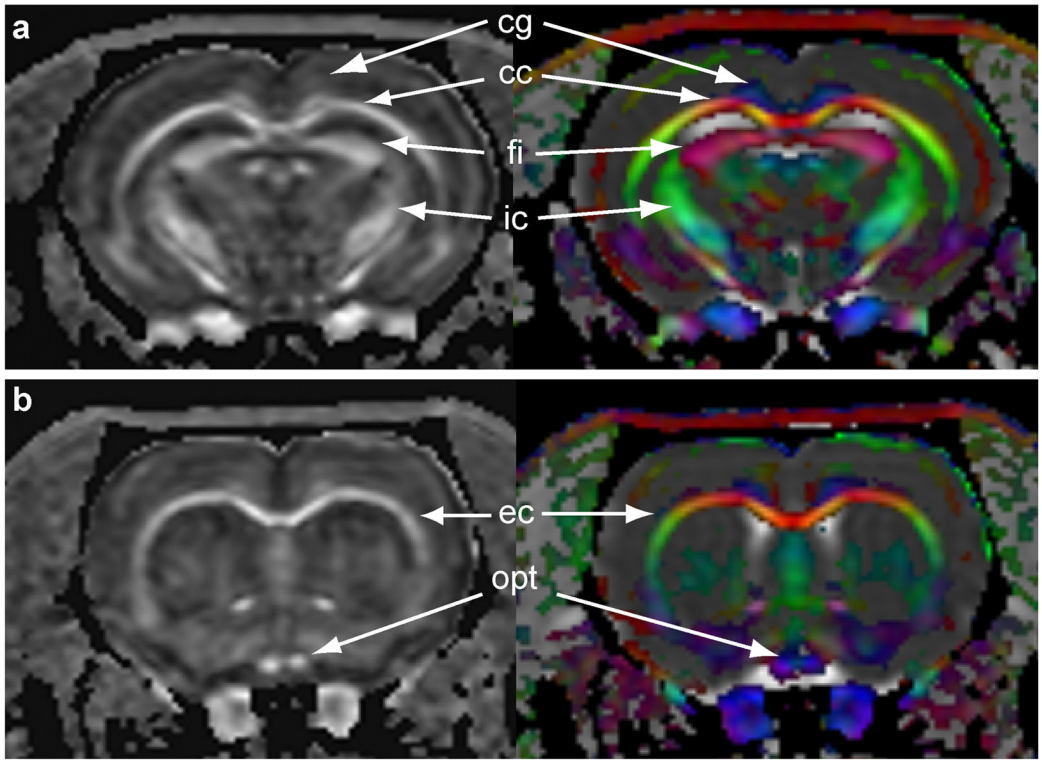

Figure 1.

FA, averaged over all the animals, with the corresponding RGB maps describing the fiber tract orientation. The RGB color-coding indicates the orientation of fibers within white matter tracts. Blue indicates fibers in the coronal plane, red indicates right and left orientation both medial and lateral, while green indicates anterior to posterior orientation. (**a**) Normal brain image taken from posterior and (**b**) anterior brain regions. The brain structures are identified and labeled using the The Rat Brain in Stereotaxic Coordinates (Paxinos and Watson, 2005): cg – cingulum; cc - corpus callosum; fi – fibria; ic – internal capsule; ec – external capsule; and opt – optic nerve.

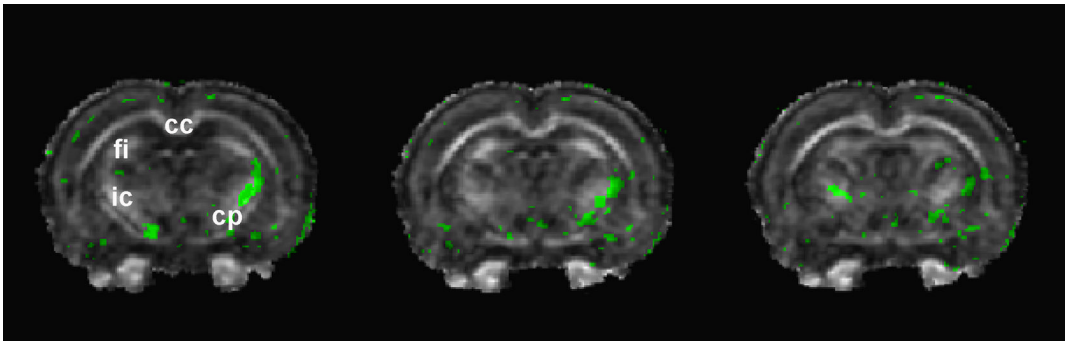

Figure 2.

Average fractional anisotropy (FA) differences (t-maps) between the brains of uninjured and six weeks spinal cord injured adult rats. Three consecutive sections (0.2 mm apart) taken from MRI scans illustrate the significant differences between combined injured and uninjured animals brain regions identified by green labels ($P < 0.05$). The following brain structures were identified and labeled using The Rat Brain in Stereotaxic Coordinates (Paxinos and Watson, 2005): cc - corpus callosum; fi – fibria; ic – internal capsule; cp – cerebral peduncle.

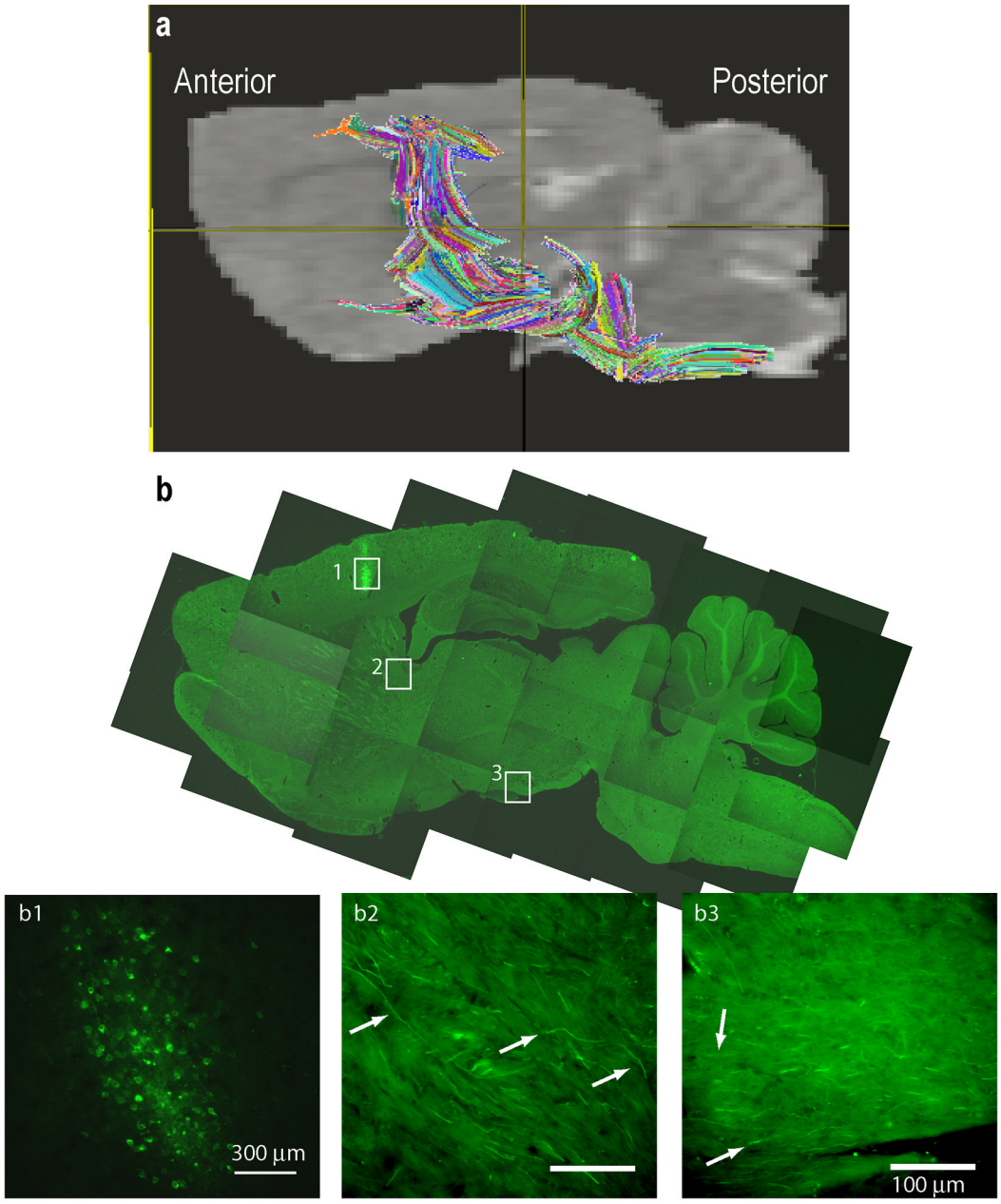

Figure 3.

a) Magnetic resonance image showing the fibers (averaged over all the animals) along the region occupied by the corticospinal tract. Colored fibers represent fiber counts based on ROIs placed along the region the CST would pass through determined by the stereotaxic atlas (Paxinos and Watson, 2005). b) Low and high magnification images of a sagittal brain section with BDA labeled CST tract. Inlet figures b1 corresponds to the BDA label cell bodies of the CST while b2, and b3 correspond to the CST fibers (identified by arrows) in the internal capsule and cerebral peduncle regions respectively. Scale bars: b1 = 300µm, b2,3 = 100µm.

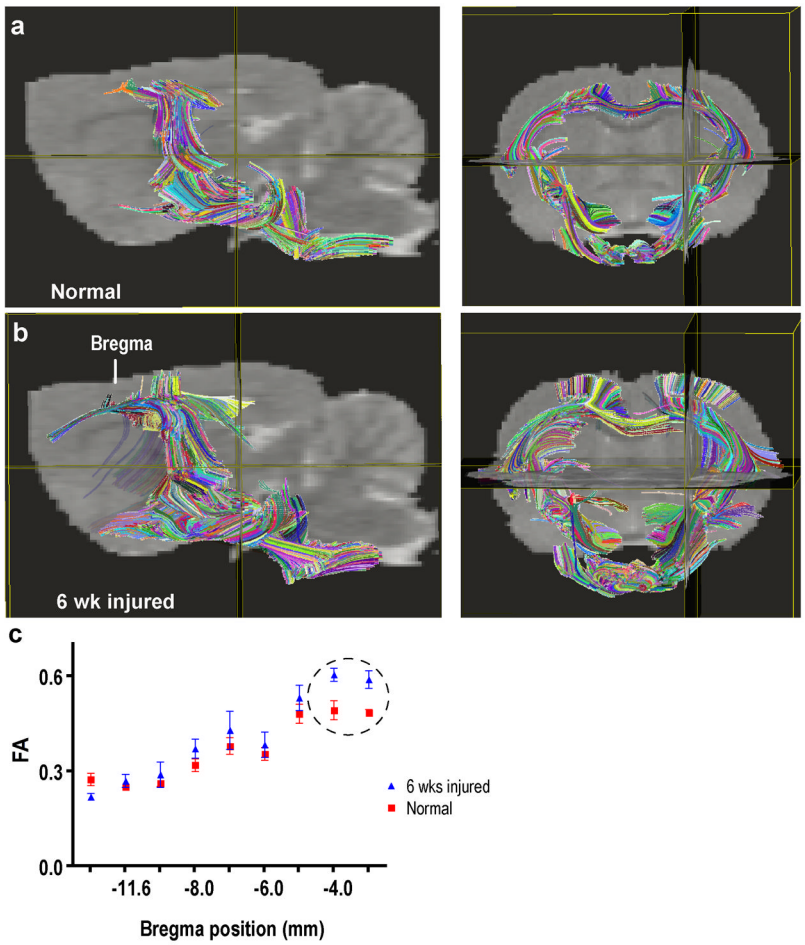

Figure 4.

DTI image comparisons of brains from normal and SCI animals. Brains from control a) and (b) SCI rat presented in both sagittal and coronal plane. (c) FA values (mean ± SD) measured at different positions along the CST. The circle in the graph represents the regions of significant difference at the level of both the internal capsule and cerebral peduncle.

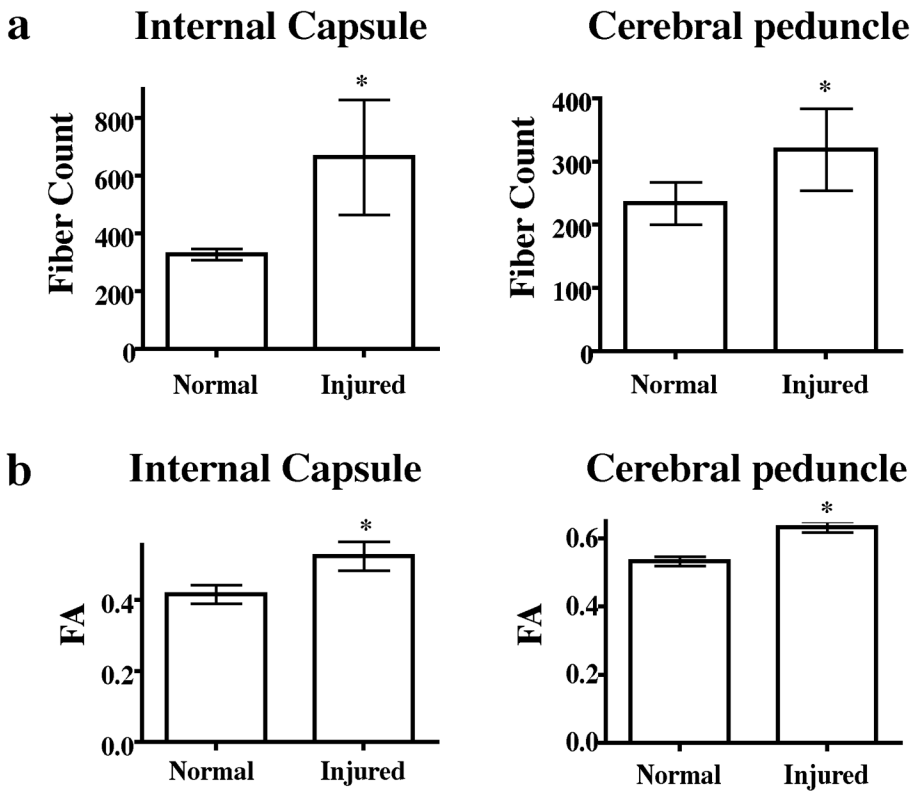

Figure 5.

Quantification of fiber counts and FA values from ROIs in internal capsule and cerebral peduncle of normal and SCI animals. A significant increase in fiber counts and FA values was detected in both structures in SCI vs naïve. “*” indicates significance at P = 0.05.

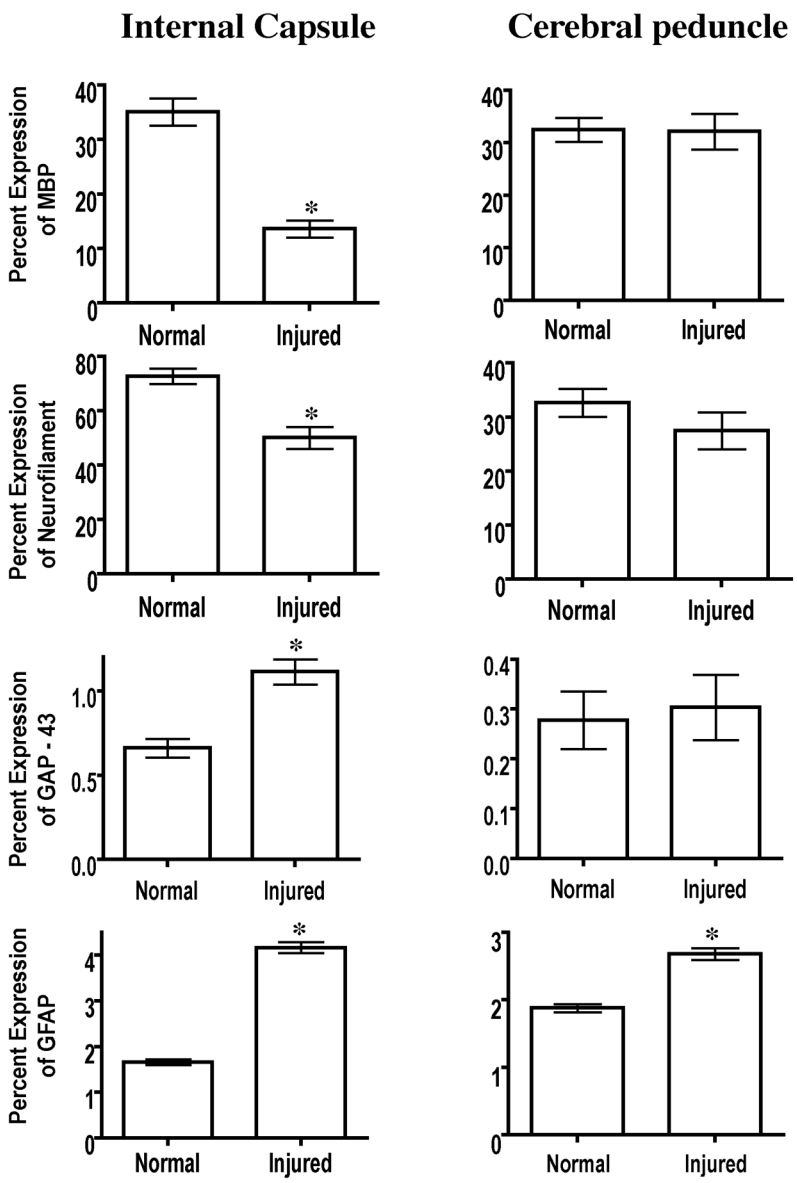

Figure 6.

Histological quantification of myelin basic protein, neurofilament-H, GAP-43 and GFAP in ROIs within the internal capsules and cerebral peduncles of naïve and injured subjects. Significance was set at P = 0.05.

Table 1

Group comparisons of DTI measures and histology between Internal Capsule and Cerebral Peduncle in naïve vs SCI animals.

Normal	Internal Capsule	Six weeks injured	*P* value
328 ± 7.992 (294–355)	Fiber counts	664 ± 81.33 (503–956)	0.0022
0.5338 ± 0.005 (0.5225–0.56)	FA	0.6333 ± 0.006 (0.62–0.65)	0.0022
0.00117 ± 0.000002 (0.00102–0.00136)	λ_l	0.00118 ± 0.000003 (0.00109–0.00127)	0.7169
0.00039 ± 0.000007 (0.000369–0.000427)	λ_t	0.00038 ± 0.000001 (0.000371–0.00043)	0.1063
72.83 ± 2.826	Percent NF-H	50.22 ± 4.040	<0.0001
35.12 ± 2.490	Percent MBP	13.69 ± 1.568	<0.0001
0.6602 ± 0.0552	Percent GAP-43	1.112 ± 0.0754	<0.0001
1.662 ± 0.0579	Percent GFAP	4.169 ± 0.1192	<0.0001
	Cerebral Peduncle		
234 ± 13.56 (206–298)	Fiber counts	319 ± 26.42 (296–447)	0.0022
0.4155 ± 0.105 (0.375–0.435)	FA	0.5229 ± 0.0167 (0.46–0.55)	0.0152
0.00124 ± 0.000006 (0.0012–0.00125)	λ_l	0.00122 ± 0.00002 (0.00118–0.00136)	0.075
0.00061 ± 0.000004 (0.000629–0.000634)	λ_t	0.00057 ± 0.000007 (0.000545–0.000629)	0.0037
32.68 ± 2.597	Percent NF-H	27.50 ± 3.386	0.1646
32.47 ± 2.270	Percent MBP	32.17 ± 3.402	0.7003
0.2780 ± 0.0575	Percent GAP-43	0.3035 ± 0.0652	0.8633
1.880 ± 0.0641	Percent GFAP	2.681 ± 0.0839	<0.0001

Values represent mean ± SEM.

Values within the parenthesis represent the range across all the animals.